EUV Interferometry of a Four-Mirror Ring-Field EUV Optical System

Kenneth A. Goldberg*[a], Patrick Naulleau[a], Phillip J. Batson[a], Paul Denham[a], Erik H. Anderson[a], Jeffrey Bokor[a,b], and Henry N. Chapman[c]

[a]Center for X-Ray Optics, Lawrence Berkeley National Laboratory, Berkeley, CA 94720
[b]EECS Department, University of California, Berkeley, CA 94720
[c]Lawrence Livermore National Laboratory, L-395, Livermore, CA 94550

ABSTRACT

At-wavelength, extreme ultraviolet interferometric measurements of a new, four-mirror, ring-field projection optical system have been made. Designed for operation at 13.4-nm wavelength with a 0.1 numerical aperture and a 26 mm field of view at the wafer, the nearly diffraction-limited wavefront quality of the system has been verified interferometrically. After assembly and alignment with visible-light interferometry, the optic was transported to Lawrence Berkeley National Laboratory where the at-wavelength testing with a phase-shifting point diffraction interferometer was performed. Measurement of the system wavefront at a number of points across the field of view reveals the optical performance of the system over its large, ring-field imaging area.

Keywords: interferometry, extreme ultraviolet lithography, EUV, point-diffraction interferometer, at-wavelength testing.

1. INTRODUCTION

High-accuracy extreme ultraviolet (EUV) interferometry[1] has recently been developed to support the fabrication of diffraction-limited projection optical systems for EUV lithography. The phase-shifting point diffraction interferometer (PS/PDI) has emerged as the design of choice for at-wavelength testing of EUV optical systems, where the wavelength is near 13.4 nm and angstrom-scale wavefront measurement accuracy and precision are required.[2,3,4]

Operating at the Advanced Light Source (ALS) synchrotron radiation facility at Lawrence Berkeley National Laboratory, PS/PDI interferometry has been used in the measurement and alignment of several small-field EUV 10× Schwarzschild objectives.[5] A new branchline of the undulator source was constructed specifically for at-wavelength testing of the Projection Optics Box (PO Box), a recently fabricated four-mirror ring-field EUV optical system which is designed to operate at 13.4-nm wavelength with 0.1 numerical aperture (NA) and 4× demagnification. The PO Box was assembled at Lawrence Livermore National Laboratory and aligned initially using visible-light interferometry.[6,7]

The PS/PDI interferometer was constructed to evaluate the system wavefront at arbitrary positions across the field of view. Measurements of the field-dependent optical performance, across the large ring-field imaging area, provide feedback for the alignment of the individual mirror elements, enabling optimal imaging quality to be achieved.

The PS/PDI design, described elsewhere,[1] has only a few critical optical components. A small pinhole in the object (reticle) plane (the *object pinhole*) produces coherent, spherical-wave illumination of the test optic. A grating beamsplitter placed between the object pinhole and the test optic creates a series of overlapping coherent beams that are focused in the image (wafer) plane. Each of these beams acquires the aberrations of the optical system via transmission. In the image-plane where the multiple beams form separable foci displaced by several microns, a patterned, opaque and transparent mask selects two adjacent beams; all other beams are blocked. One of the two beams is passed through a relatively large open window in the mask and propagates on to reach an EUV CCD camera. The second beam is focused onto a pinhole smaller than the diffraction-limited resolution of the test optic (the *reference pinhole*) producing a spherical reference beam. The two beams overlap at the CCD where they produce an interference pattern. Analysis of the interferogram reveals the path length difference between the test beam and the spherical reference, and hence contains the wavefront aberrations of the test optic.

The measured system wavefronts represent the combined, additive contributions of the individual mirrors' surface figures and their multilayer optical coatings. Past experiments with EUV 10× Schwarzschild objectives have revealed the high-accuracy

*Correspondence: Email: KAGoldberg@lbl.gov; Telephone: 510-495-2261; Fax: 510-486-4550

of at-wavelength PS/PDI testing of EUV optics,[1] and have demonstrated its unique capability for investigating issues related to the multilayer coatings.[8] In addition to the wavefront measurements presented in this article, the PS/PDI is uniquely suited to characterize flare and the system's chromatic bandwidth. Also of high interest, the EUV PS/PDI can be used to evaluate the performance of high-accuracy visible light interferometry used during the fabrication of the individual mirror elements and during the alignment of the assembled system.[7]

2. SYSTEM CONFIGURATION

The large field of view (26-mm arc in the image/wafer plane, 104-mm in the object/reticle plane) posed a significant engineering challenge for the construction of the interferometer: wavefront measurements must be made at field points spanning the entire field of view. Owing to the geometry and narrow tolerances of the glancing-incidence optics in the beamline illumination system, it proved easier to position the optical system under a stationary beam focused in the object (reticle) plane than to keep the optic stationary and adjust the position and angle of the beam.

2.1. Main Chamber

Figure 1 schematically shows the interferometer configuration including the PO Box, the beam path and many of the essential optical and mechanical components. The entire system operates at a vacuum base pressure of 10^{-9} Torr in the beamline where differential ion pumps are used, and 10^{-7} Torr in the main interferometry chamber where pumping is performed by a 1,600 l/sec turbo pump.

To facilitate installations and maintenance, the main interferometry chamber rests permanently on an air palette, which, when activated, is used to float the chamber into a clean room located adjacent to the beamline. The chamber has a removable lid that makes it possible for the PO Box to be loaded and unloaded with a crane.

A temperature-controlled enclosure is constructed around the interferometry chamber and the pre-focusing beamline optics. Temperature is continuously monitored and recorded at 29 separate locations on the PO Box. Aided by the long thermal time constant of the system when at vacuum, the thermal control system maintained a constant temperature of 20.45 C ± 0.02 C over several days.

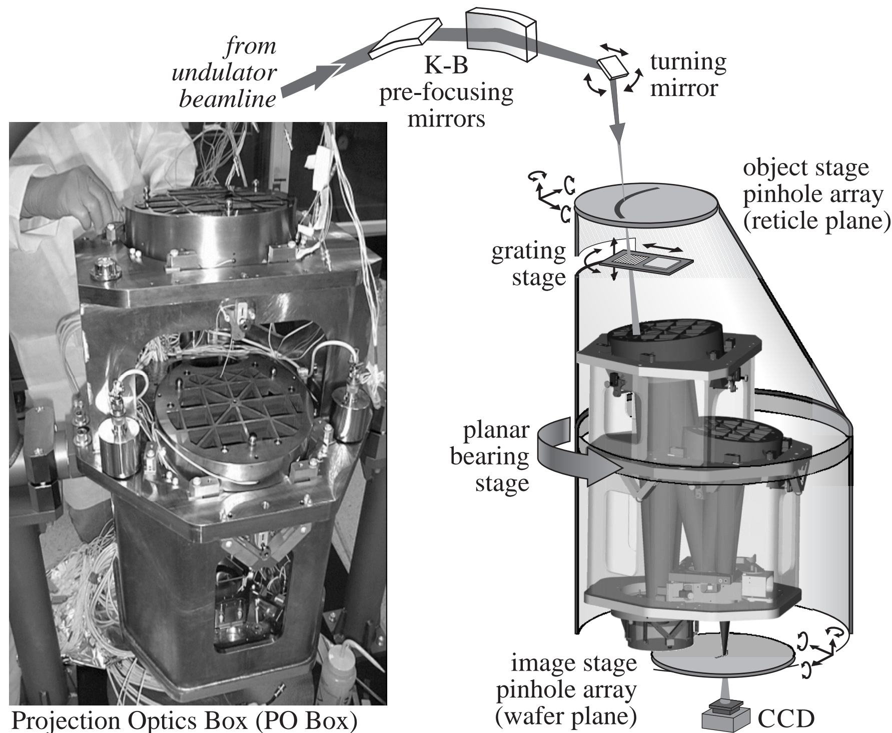

Figure 1. (Left) The PO Box. **(Right)** Critical optical components and stages of the PS/PDI configured for measurement of the PO Box.

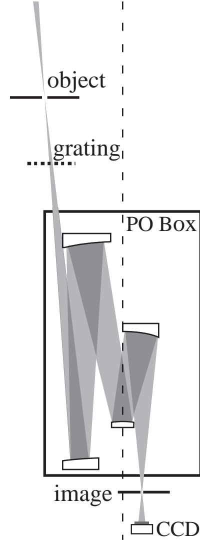

Figure 2. PO Box interferometer configuration schematic.

Table 1. Interferometer and PO Box specifications.

input (object-side) NA	0.025
output (image-side) NA	0.1
input beam angle	5.435°
radius at center of field-arc	
object side	211 mm
image-side	52.75 mm
width of field-arc (image plane)	26 mm
mean object pinhole diameter	200 nm
mean reference pinhole diameter	~100 nm
object-to-grating distance	75 mm
grating pitch	50 µm
image-to-CCD distance	80 mm
CCD area	2.54 cm
moving components	object, PO Box, image
stationary components	grating, CCD
temperature	20.45 C ± 0.02 C

2.2. Interferometry Beamline

The interferometry beamline has been described elsewhere.[9,10] It consists of an undulator radiation source paired with a high-efficiency monochromator that provides adjustable bandwidth ($\Delta\lambda/\lambda$) between 1/200 and 1/1000, much narrower than the bandwidth of the optical coatings in the PO Box. The throughput of the illumination system depends critically on the quality of the pre-focusing optics and their ability to deliver the maximum amount of available light though sub-half-micron object pinholes. A two-mirror, glancing-incidence Kirkpatrick-Baez (KB) system was engineered with eight Picomotor-driven actuators to enable *in situ* bending adjustment of the mirrors. A thin, fluorescent crystal is placed in the focal plane of the KB where a CCD microscope provides real-time feedback with one-micron resolution. Adjustable degrees of freedom include the mirror tilts, the bending moments applied to each end, and a twist actuator. Nearly-diffraction-limited focusing with a 4-µm by 7-µm spot size is routinely achieved. A removable "45°" Mo/Si-multilayer-coated turning mirror inserted after the KB system directs the beam downward at the proper angle for the PO Box. The turning mirror is held on an adjustable and translatable gimbals mount to enable beam steering.

2.3. Stages

The PO Box is supported by three points affixed to an annular planar bearing stage (PBS) that circumscribes the optic near its center of gravity. The stage consists of two annular rings: a mobile ring rides above a stationary ring that is vibrationally decoupled from the vacuum chamber. Between the two rings are approximately 4,800 ball bearings captured in a teflon retainer. Three arms, positioned at tangents to the ring bearing, and placed at 120° intervals, are attached to the mobile upper part of the PBS. The three arms are individually driven by dc-motors outside of the vacuum chamber. The arms pass into the chamber through bellows. The arm positions are monitored against Heidenhein scales located outside of the chamber; the scales are referenced to rigid rods coupled through separate bellows into the chamber, and attached to the stationary lower portion of the PBS. The symmetric, three-arm drive mechanism simplifies rotation of the PBS and enables ±15° of motion. Following a mathematical algorithm, differential motion of the three arms enables arbitrary lateral or rotational motion of the system. As constructed, the stage has sub-micron long-term stability and micron-scale repeatability for large moves.

Independent object- and image-plane stages hold and position the wafers that contain the pinhole arrays. These stages are rigidly mounted to the same planar bearing structure that supports the PO Box; therefore the test optic and the stages move together as a single unit, maintaining fixed relative positions of the pinhole arrays in the conjugate planes. The two similar flexure stages are Picomotor driven with six degrees of freedom over a small range of motion. Linear variable differential transformer (LVDT) and capacitance micrometers provide sub-10-nm motion resolution. In practice, the object mask position is adjusted only initially to bring the pinhole array into alignment with the field point positions. During measurement of the system wavefront across the field of view, the object mask position is held fixed, serving as a position reference; the image-stage is moved as required to bring the image-plane pinholes into the conjugate positions. Alignment features in the object and image masks eliminate the beam position ambiguity within the array.

The grating beamsplitter is held on a stage supported by the stationary ring of the PBS, and it remains stationary with respect to the illuminating beam. The grating stage moves with four degrees of freedom: insertion and extraction from the beam, rotation about the grating's center, longitudinal motion to control the beam separation in the image plane, and translation perpendicular to the grating rulings for phase-shifting.

2.4. CCD Detector

An EUV-sensitive 1024 × 1024 pixel CCD camera is placed approximately 80 mm below the image-plane, in a small isolatable vacuum chamber. The telecentricity of the optical system means that the plane of the CCD, parallel to the ground, is always normal to the central ray of the transmitted light. While the CCD remains stationary, the beam footprint moves with the lateral displacement of the PO Box. Because the optical design has rotational symmetry through the arc of the field of view, rotation (axial motion) of the PO Box produces no motion of the beam footprint on the detector.

2.5. Object- and Image-Plane Pinhole Arrays

To define the field positions where wavefront measurements must be made, two similar arrays of pinholes were fabricated for the two conjugate planes. The object pinhole array which occupies the mask plane consists of a pattern of 21 pinholes and four alignment marks at each of the 45 field points The pinhole spacing in a square 5 × 5 array is 90 µm. Within the arrays, a range of pinhole sizes was patterned so that the appropriate pinhole size could be determined and used. The image plane mask has a relative 4× demagnification in scale, and a pattern containing reference pinholes and transparent windows. At each of the 45 field points, a 6×8 array of PS/PDI window-pinhole features was used, again giving a range of pinhole sizes. Redundant pinholes can be used in series to reduce measurement uncertainties. Each window has two reference pinholes and is spaced at 50 µm from adjacent windows. Interspersed between the windows are pinhole pairs designed for two-pinhole null test measurements, used for calibrating the interferometer.[1,4]

3. WAVEFRONT MEASUREMENTS

In addition to the characterization of the system wavefront, which enables the prediction of imaging performance, interferometric wavefront measurements can be combined with an alignment procedure to improve overall wavefront quality. An alignment algorithm developed at Lawrence Livermore National Laboratory specifies up to 45 field points, arranged in nine columns, where measurements are to be made.[11] Implementation of the alignment procedure and discussion of the intermediate results will be presented in a subsequent paper.

The alignment procedure provides more than just feedback on the relative positions of the four mirrors of the PO Box: of equal importance are the conjugate positions used in the measurement. Attached to the frame of the PO Box, capacitance micrometers are used to measure the longitudinal object stage position at three points. *In situ* distortion measurements performed during the visible-light alignment help to determine the optimal stage position. This information can be transferred to the EUV interferometer so that measurements will be performed in the same conjugate positions in both systems. Once positioned, the object stage is generally held stationary: the image-plane stage is rotated and translated to align the image-pinhole array with the conjugate positions dictated by the object array. For the EUV interferometry, the relative alignment of the image-plane array was achieved to within five microns across the measured field of view.

Wavefront measurements made across the field of view were always performed within an 8-hour period. Once the relative positions of the object- and image-plane pinhole arrays were well known, measurements required from five to eight minutes per point. Using control software that keeps track of the beam position within the object-plane pinhole array as the optic is rotated and translated across the field of view, the system could be steered from one field point to an adjacent point in under a minute. Twenty-second exposure times were typical for the data collection images. The observed fringe contrast was usually above 50 percent.

Interferometric wavefront measurements confirm the nearly diffraction-limited wavefront quality of the PO Box. The measurements presented here represent the final, optimized state of the PO Box, following two alignment iterations and wavefront characterizations across the field of view. Owing to a mechanical restriction in the PBS, the PO Box could be rotated to reach only 40 of the 45 pre-defined field points. Mask fabrication difficulties further restricted the number of measurable field points to 35. System wavefront measurements of those 35 points are presented in this section and in Figures 3-6.

A combination of phase-shifting and static interferogram analysis is used to produce the wavefront measurements. Owing to the high fringe density (about 73 fringes across 0.1 NA) the Fourier-transform method[12] of static interferogram analysis can

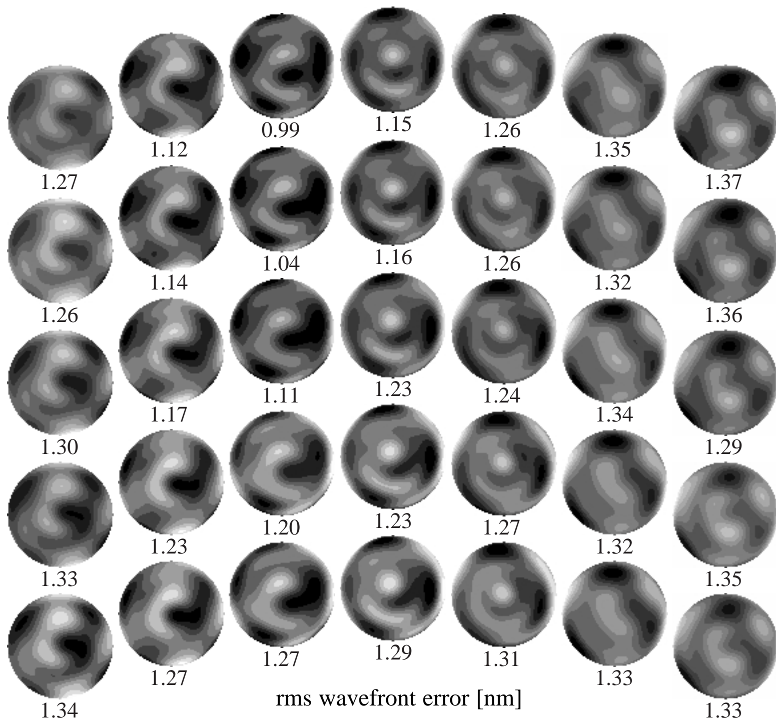

Figure 3. Wavefront phasemaps measured at 35 points across the field of view. Shown are reconstructions from 37-term Zernike polynomial fitting and the rms magnitude of the wavefront error in nm. Gray levels represent steps of 0.75 nm.

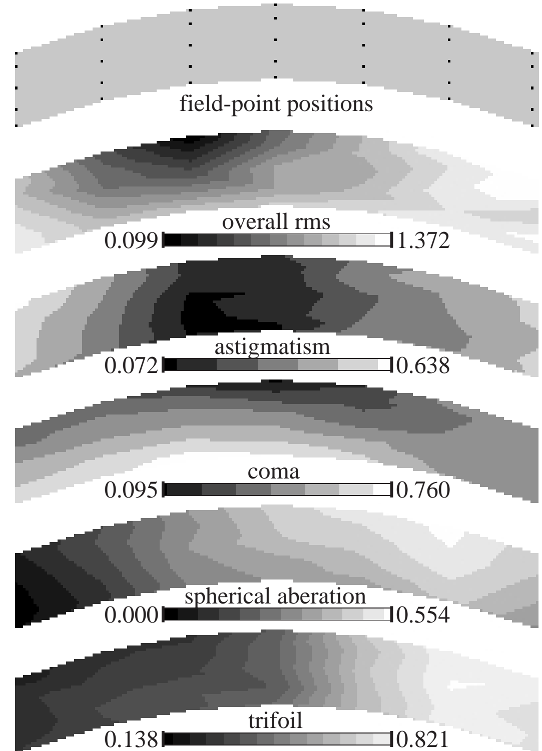

Figure 4. Variation of the overall rms wavefront aberration magnitude and the rms magnitude of individual aberration components across the field of view. **(Top)** The relative positions of the field points within the field are shown to scale. Intermediate values are interpolated.

be used with high accuracy. The Fourier-transform method was implemented with a circular, 35-cycle-radius, third-order Butterworth filter in the spatial frequency domain to retain most of the available spatial frequency content in the raw data. In these measurements, the high-spatial-frequency cutoff is set physically by the 3-µm size of the square window in the image plane.

Following the interferogram analysis, the raw wavefront data is fit to a set of 37 Zernike polynomials using a Gram-Schmidt orthogonalization procedure.[13] The measurement- and position-dependent piston, tilt, and defocus terms are subtracted from the wavefront before subsequent analysis. A systematic coma component is also subtracted from the raw wavefront to compensate for a geometric path-length difference between the test and reference beams.[14,15]

Field-dependent variation of the measured system wavefront, and the variation of the individual wavefront aberration components are shown in Figures 3, 4, and 5 respectively. Figure 6 shows the wavefront measurement from a single field point: the point with the largest arc radius, in the first column to the left of center.

All of the measured wavefront data are smoothly and slowly varying across the field of view. Given the facts that the data are compiled from 35 largely uncorrelated measurements, made over a six-hour period, with different pairs of conjugate pinholes, and subtending different regions of the CCD detector, the data attest to the exceptionally high precision of the interferometer. Careful investigation of the measurements made across the field of view, in particular the inspection of the raw wavefront data, reveals that the individual hills and valleys in the phasemaps are attributable to features on the individual mirrors within the PO Box. As different field points are illuminated, the beam footprint moves across mirrors M1, M2, and M4 at different rates, and in different directions; the features of the spherical, on-axis mirror, M3, appear fixed with respect to the borders of the wavefront. The deterministic motion of these localized features assures us that they are real, and are unrelated to measurement noise.

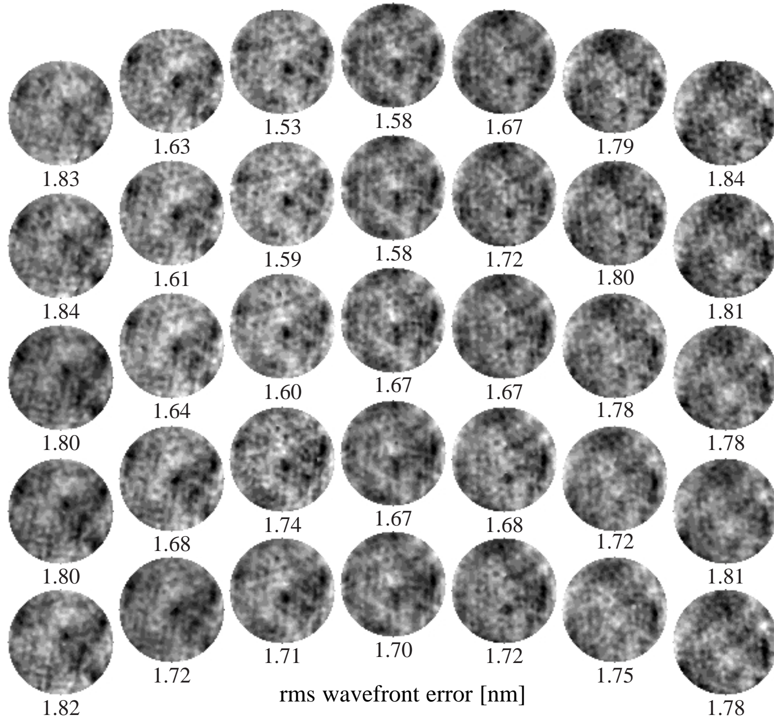

Figure 5. Wavefront phasemaps measured at 35 points across the field of view. Shown is higher spatial frequency content than is contained within 37-term Zernike polynomial reconstructions and the associated rms magnitude. Gray levels represent steps of 1.0 nm.

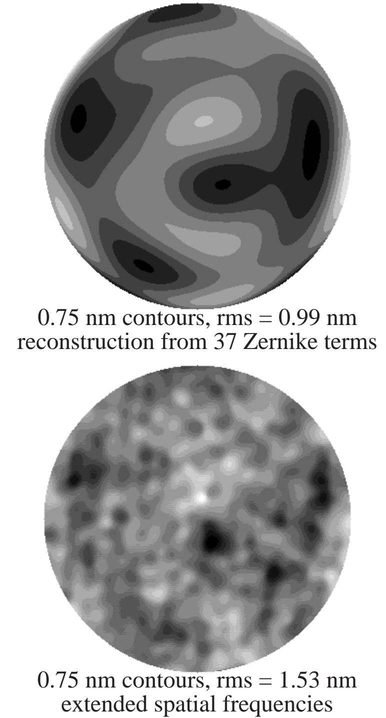

Figure 6. One wavefront measurement form the field position at the largest radius of the arc, in the first column to the left of center. **(Top)** reconstruction from a 37-term Zernike polynomial fit. **(Bottom)** Raw wavefront data on which the Zernike fit is based.

4. CONCLUSION

At-wavelength extreme ultraviolet interferometric testing has been performed on a four-mirror, ring-field projection optical system, confirming its nearly diffraction-limited performance across a large field of view. Wavefront measurements made with the EUV phase-shifting point diffraction interferometer at a large number of points within the field of view were used to iteratively test and align the PO Box. Across the field of view, the smooth variation of the system wavefront and the individual aberration components attests to both the high surface figure quality of the optical elements in the PO Box and to the high-precision of the EUV PS/PDI interferometer. EUV alignment, flare measurement, chromatic bandwidth testing, and comparisons with visible-light and EUV shearing interferometries will be addressed in subsequent articles.

5. ACKNOWLEDGMENTS

The authors are grateful for the hard work and contributions of the CXRO engineers and staff including Keith Jackson, Kevin Bradley, Brian Hoef, David Richardson, Farhad Salmassi, M. Gideon Jones, Nord Andreson, Lon Amerman, René Delano, Matt Bjork, James Comins, Douglas Lahti, and Kevin Geary. We are also indebted to Erik Anderson for electron beam lithography support and development of the pinhole arrays, and to Dino Cirlo for wafer processing. Technical assistance with the POB alignment was provided by Nhan Nguyen. This research has been supported by the Extreme Ultraviolet Limited Liability Company (EUV LLC), the DARPA Advanced Lithography Program, and by the Office of Basic Energy Sciences of the U.S. Department of Energy.

6. REFERENCES

1. P. Naulleau, K. A. Goldberg, S. Lee, C. Chang, C. Bresloff, P. Batson, D. Attwood, and J. Bokor, “Characterization of the accuracy of EUV phase-shifting point diffraction interferometry,” in *Emerging Lithographic Technologies II*, Y. Vladimirski, ed., *Proc. SPIE* **3331**, 114-23 (1998).

2. H. Medecki, E. Tejnil, K. A. Goldberg, and J. Bokor, "Phase-shifting point diffraction interferometer," *Optics Letters* **21** (19), 1526-28 (1996).

3. H. Medecki, U.S. Patent 5,835,217: "Phase-shifting point diffraction interferometer," Nov. 1998.

4. P. P. Naulleau, K. A. Goldberg, S. H. Lee, C. Chang, D. Attwood, and J. Bokor, "Extreme-ultraviolet phase-shifting point-diffraction interferometer: a wave-front metrology tool with subangstrom reference-wave accuracy," *Applied Optics*, **38** (35), 7252-63 (1999).

5. K. A. Goldberg, P. Naulleau, and J. Bokor, "EUV interferometric measurements of diffraction-limited optics," *Journal of Vacuum Science and Technology* **B**, **17** (6), 2982-86 (1999).

6. J. S. Taylor, G. E. Sommargren, D. W. Sweeney, R. M. Hudyma, "The fabrication and testing of optics for EUV projection lithography," in *Emerging Lithographic Technologies II*, Y. Vladimirski, ed., *Proc. SPIE* **3331**, 580-90 (1998).

7. D. Tichenor *et al*., "EUV Engineering Test Stand," *these proceedings.*

8. K. A. Goldberg, P. Naulleau, S. H. Lee, C. Chang, C. Bresloff, R. Gaughan, H. N. Chapman, J. Goldsmith, and J. Bokor, "Direct comparison of EUV and visible-light interferometries," in *Emerging Lithographic Technologies III*, Y. Vladimirski, Ed., *Proc. SPIE* **3676**, 635-42 (1999).

9. D. T. Attwood, P. Naulleau, K. A. Goldberg, E. Tejnil, C. Chang, R. Beguiristain, P. Batson, J. Bokor, E. M. Gullikson, M. Koike, H. Medecki, and J. H. Underwood, "Tunable coherent radiation in the soft x-ray and extreme ultraviolet spectral regions," *IEEE Journal of Quantum Electronics* **35** (5), 709-20 (1999).

10. E. Tejnil, K. A. Goldberg, S. H. Lee, H. Medecki, P. J. Batson, P. E. Denham, A. A. MacDowell, and J. Bokor, "At-wavelength interferometry for EUV lithography," *Journal of Vacuum Science and Technology B*, **15** (6), 2455-2461 (1997).

11. H. N. Chapman and D. W. Sweeney, "A rigorous method for compensation selection and alignment of microlithographic optical systems," *Proc. SPIE* **3331**, 102-113 (1998).

12. Bone, D. J., H.-A. Bachor, and R. J. Sandeman, "Fringe-pattern analysis using a 2-D Fourier transform," *Applied Optics*, **25** (10), 1653-60 (1986).

13. D. J. Fischer, J. T. O'Bryan, R. Lopez, and H. P. Stahl, "Vector formulation for interferogram surface fitting," *Applied Optics,* **32** (25), 4738-43 (1993).

14. K. A. Goldberg, "Extreme Ultraviolet Interferometry," doctoral dissertation, Department of Physics, University of California, Berkeley, 1997.

15. K. A. Goldberg, "Testing extreme ultraviolet optical systems at-wavelength with sub-angstrom accuracy," in Trends in Optics and Photonics Vol. 24, *Fabrication and Testing of Aspheres*, A. Lindquist, M. Piscotty, and J. S. Taylor, Eds. (Optical Society of America, Washington, DC), 1999.